Internal resonance with commensurability induced by an auxiliary oscillator for broadband energy harvesting

Liuyang Xiong, Lihua Tang, and Brian R. Mace

Citation: Applied Physics Letters **108**, 203901 (2016); doi: 10.1063/1.4949557
View online: http://dx.doi.org/10.1063/1.4949557
View Table of Contents: http://scitation.aip.org/content/aip/journal/apl/108/20?ver=pdfcov
Published by the AIP Publishing

Internal resonance with commensurability induced by an auxiliary oscillator for broadband energy harvesting

Liuyang Xiong, Lihua Tang,[a] and Brian R. Mace
Department of Mechanical Engineering, University of Auckland, 20 Symonds Street, Auckland 1010, New Zealand

(Received 8 March 2016; accepted 3 May 2016; published online 16 May 2016)

An internal resonance based broadband vibration energy harvester is proposed by introducing an auxiliary oscillator to the main nonlinear harvesting oscillator. Compared to conventional nonlinear energy harvesters, the natural frequencies of this two-degree-of-freedom nonlinear system can be easily adjusted to be commensurable which will result in more resonant peaks and better wideband performance. Experimental measurements and equivalent circuit simulations demonstrate that this design outperforms its linear counterpart. In addition to the open-circuit voltage, the optimal resistance to obtain the maximum power is determined. Nearly 130% increase in the bandwidth is achieved compared to the linear counterpart at an excitation level of 2 m/s^2. The findings provide insight for the design of a broadband energy harvester when there is nonlinearity and internal resonance. *Published by AIP Publishing*. [http://dx.doi.org/10.1063/1.4949557]

The design of a piezoelectric vibration energy harvester (PVEH) to capture waste energy for small, self-sustained wireless electronic devices has received much attention in recent years.[1–5] Conventional PVEHs have to work in a limited resonant frequency range, which limits the harvesting efficiency under broadband ambient vibrations. To remedy this key issue of conventional PVEHs, tuning mechanisms are employed to alter the natural frequency of the harvester to match the excitation frequency.[6,7] The disadvantages are complexity in design and required power for active tuning. The multi-modal method is also proposed for broadband purposes.[8,9] Shahruz[10] and Ferrari *et al.*[11] used an array of cantilever beams with different frequencies to achieve wide bandwidth but at the cost of reducing the power density. To actualize multi-modal energy harvesting with two close resonances in one structure, some researchers exploited multi-modal piezoelectric structures by attaching an additional oscillator or dynamic magnifier.[12,13] Erturk *et al.*[14] proposed an L-shaped beam-mass system as an alternative configuration to a cantilevered beam. Tang and Yang[15] derived a general multiple-degree-of-freedom (MDOF) piezoelectric energy harvesting model which could achieve close resonant peaks by properly adjusting auxiliary oscillators attached to a main harvesting oscillator. Wu *et al.*[16] further developed a "cut-out" 2DOF harvester with a secondary beam enclosed within the main beam, which achieved two close resonances both with significant power amplitudes. Other than a tuning mechanism and the multi-modal technique, introducing nonlinearities into a PVEH is another promising solution, as multiple stable equilibriums and the bending of response curves can be employed to cover a larger frequency range.[17,18] Magnetic interaction is the most common approach to introduce the nonlinearity. Erturk and Inman[19] pointed out that the large-orbit solution resulting from interwell oscillations of bistable PVEHs can yield substantially larger power output over a wider bandwidth. Cottone *et al.*[20] demonstrated the superior performance of stochastic resonance in a bistable PVEH under ambient white-noise vibrations. Stanton *et al.*[21] proposed a mono-stable harvester with the tip magnet oscillating between two fixed magnets, in which both the hardening and softening responses can be observed by tuning the magnets. In addition to nonlinear external resonance with only softening or hardening properties, internal resonance is a typical phenomenon in nonlinear MDOF vibrating systems which will result in double jumping. Chen *et al.*[22] investigated the effects of internal resonances of two elastically connected cantilevers with nonlinear boundary conditions, and their findings implied that internal resonance could provide another opportunity to broaden the working frequency range for energy harvesting purposes. Chen and Jiang theoretically studied this mechanism in a snap-through electromagnetic energy harvester.[23] Lan *et al.*[24] applied dynamic instability in a vertical beam with a tip mass and claimed the benefit for large voltage output from energy transfer of the internal resonance. Xu and Tang[25] studied a cantilever-pendulum design to achieve multi-directional energy harvesting by using internal resonance induced energy interchange between beam bending and various pendulum swing modes.

An L-shaped beam structure has been acknowledged as a simple case to realize internal resonance.[14] Cao *et al.*[26] explored an L-shaped beam for energy harvesting analytically and numerically. Engel[27] attempted to implement this idea experimentally, but the internal resonance behavior became noticeable only for very large amplitude excitations. The limitation is that the geometric nonlinearity is generally too weak to show significant influence on the dynamic responses. Magnetic interaction can introduce a strong nonlinearity. However, the commensurability of the first two natural frequencies is difficult to achieve with a typical cantilever-based nonlinear PVEH structure,[15,20] in which a piezoelectric cantilever carrying a magnetic tip mass interacts with a fixed magnet on the frame.

This letter introduces an auxiliary beam to the typical nonlinear PVEH, which exhibits the strong nonlinearity of

[a]Author to whom correspondence should be addressed. Electronic mail: l.tang@auckland.ac.nz

magnetic interactions and meanwhile the first two natural frequencies of the derived linear system can easily be tuned to be commensurable with 2:1 ratio. For such a configuration, rich nonlinear behaviors are revealed, including multiple stable solutions, double jumping, and energy exchange between modes. With the derived equivalent circuit model and identified parameters, the nonlinear dynamics and energy harvesting performance are simulated and verified by experiment.

Figure 1(a) depicts the proposed PVEH based on internal resonance, and Figure 1(b) shows the experimental system. The main beam is bonded with two piezoelectric transducers (Smart Materials Corp., model: M2814P2) near the clamped end and carries a magnetic tip mass. The nonlinear restoring force is introduced by the magnet fixed on the frame. An auxiliary linear oscillator is introduced to tune commensurability. m_1 and m_2 are the effective masses of the main piezoelectric beam and the auxiliary beam with stiffness k_1 and k_2, respectively. η_1 and η_2 are the corresponding damping coefficients. The motions of the two masses relative to the frame are described by displacements u_1 and u_2. The electrical domain is characterized by resistance R_L, capacitance $C_p = 50$ nF of the piezoelectric transducers, electromechanical coupling coefficient θ, and the electric voltage output $v(t)$. The governing equations of the nonlinear 2DOF system subjected to base excitation u_0 can be described by

$$\begin{cases} m_1\ddot{u}_1 + \eta_1\dot{u}_1 + \eta_2(\dot{u}_1 - \dot{u}_2) + k_1u_1 + k_2(u_1 - u_2) \\ \quad -F_{\text{magv}} + \theta v(t) = -m_1\ddot{u}_0 \\ m_2\ddot{u}_2 + \eta_2(\dot{u}_2 - \dot{u}_1) + k_2(u_2 - u_1) = -m_2\ddot{u}_0 \\ R_LC_p\dot{v}(t) + v(t) - \theta R_L\dot{u}_1 = 0, \end{cases} \tag{1}$$

where the nonlinear force between the two repulsive magnets can be expressed using the dipole-dipole model[20]

$$F_{\text{magv}} = -\frac{3\tau M_1M_2}{2\pi}\frac{u_1 + \Delta_1}{\left[(u_1 + \Delta_1)^2 + D_1{}^2\right]^{2.5}}, \tag{2}$$

where $M_1 = M_2 = 0.154$ A m^2 are the effective moments of the magnetic dipoles and $\tau = 4\pi \times 10^{-7}$ T m/A is the vacuum permeability. The distance D_1 should be calculated from center to center, that is, $D_1 = D_0 + h$, where D_0 is the distance between the facing surfaces of the two magnets and $h = 0.005$ m is the thickness of the magnet. Δ_1 is the misalignment of initial positions of magnets in the vertical direction (Figure 1(a)). This disturbs the symmetry of the magnetic field. There may exist internal resonance if the two natural frequencies of the derived linear system are near the ratio 2:1 by varying D_0 and Δ_1.

An equivalent circuit model of the proposed system is established by considering the electrical-mechanical analogy in the governing equations (Figure 2). Force, mass, flexibility and damping in the mechanical domain are equivalent to the voltage, inductance, capacitance and resistance, respectively. Therefore, the voltage sources V_1 and V_2, inductors L_1 and L_2, capacitors C_1 and C_2, and resistors R_1 and R_2 in the equivalent circuit (Figure 2) can be obtained by

$$\begin{aligned} &L_1 = m_1, \quad L_2 = m_2, \quad R_1 = \eta_1, \quad R_2 = \eta_2, \\ &C_1 = 1/k_1, \quad C_2 = 1/k_2, \\ &V_1 = -m_1\ddot{u}_0, \quad V_2 = -m_2\ddot{u}_0. \end{aligned} \tag{3}$$

The nonlinear magnetic force F_{magv} is modeled as a behavioral voltage source V_m. The electromechanical coupling coefficient is equivalent to an ideal transformer with the winding ratio 1:θ. These parameters are determined from the experimental rig for simulations, and then experimental measurements are compared to simulation results. System parameters can be identified following a procedure similar to that used by Tang and Yang.[4] Subsequently, equivalent circuit parameters are obtained by the electrical-mechanical analogy and are shown in Table I.

A sinusoidal excitation to provide an acceleration of $a = 2$ m/s^2 and a sweep rate of 0.02 Hz/s is used. Frequency responses of the open circuit voltage are recorded in terms of the root-mean-square (RMS) value. If the fixed magnet is removed, the system will degrade to a conventional linear 2DOF harvester. For undamped free vibrations, the natural frequencies ω_1 and ω_2 of this 2DOF system are such that

$$\omega_{1,2}^2 = \frac{(m_1 + m_2)k_2 + m_2k_1 \mp \sqrt{\left[(m_1 + m_2)k_2 + m_2k_1\right]^2 - 4m_1m_2k_1k_2}}{2m_1m_2}. \tag{4}$$

Figure 3(a) shows the frequency response curve of the linear 2DOF harvester. According to Equation (4), the first two natural frequencies of the linear model are $\omega_1 = 13.59$ Hz and $\omega_2 = 27.89$ Hz, which is validated by experiment (Figure 3(a)) and simulation (Figure 3(b)).

With the magnetic interaction introduced, the linear stiffness of the nonlinear 2DOF system is slightly changed by the linear part of the magnetic force. Thus, the two natural frequencies of the derived system can be fine-tuned to be nearly commensurable with 2:1 ratio and thus 2:1 internal resonance occurs. The frequency response of the nonlinear model under internal resonance in experiment is shown in Figure 4(a). Typical internal resonance phenomenon occurs with the magnet arrangement with $D_0 = 6.7$ mm and $\Delta_1 = 2.5$ mm. The second natural frequency of the derived system is nearly twice the first natural frequency (one at around 13.5 Hz and the other at around 27 Hz). Different from the normal two single resonance peaks for the linear system, four resonance peaks exist, leading to broader bandwidth with little reduction in response magnitude (Figure

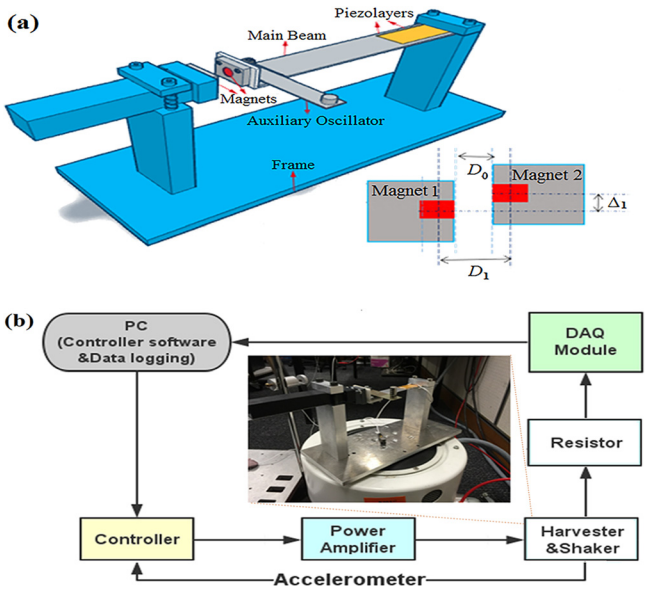

FIG. 1. (a) Schematic of proposed nonlinear PVEH with auxiliary oscillator and (b) testing setup.

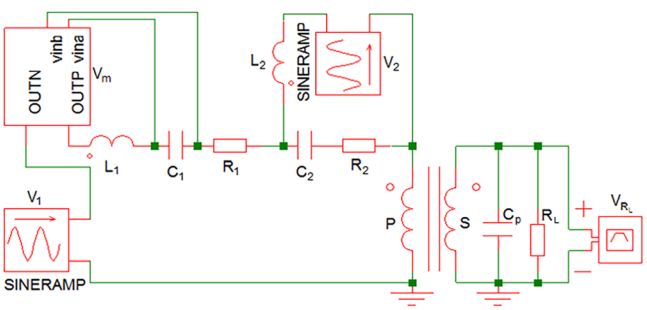

FIG. 2. Equivalent circuit representation of proposed nonlinear PVEH.

4(a)). Figure 4(b) shows the frequency response obtained by simulation. Despite the small differences in the magnitudes of the peaks, the simulations predict the same trends of nonlinear behavior as the experiments. Four peaks arising from nonlinear internal resonance are evident. The discrepancy in the magnitude of the output is probably due to the change of damping in the experiment with the magnetic force introduced, and the rotations at the free ends of the main beam, which are not taken into account in the simulations.

Samples of the steady state responses for excitations at specific frequencies are recorded in the experiments to further investigate the harmonic components in the response

TABLE I. Identified system parameters.

Parameter	Main beam	Auxiliary beam
$m_{1,2}$(g)	28.96	16.03
$k_{1,2}$ (N m^{-1})	666.29	153.85
$\eta_{1,2}$ (N s m^{-1})	0.05	0.014
θ (N V^{-1})	0.00022	/

spectrum. Figures 5(a) and 5(c) show the frequency spectra under off-resonant excitation of 8 Hz and 24 Hz. Since the system is excited harmonically far away from the first and second resonances, only one peak having the same frequency as the external excitation is evident. From Figure 5(b), it can be seen that an additional peak near the second natural frequency appears when the system is excited at 13.5 Hz, close to the first resonance. Excitation around one resonance frequency is coupled through the internal resonance to a large response at the other resonance frequency. Note also that the response is much larger than when excited off-resonance (Figures 5(a) and 5(c)). Figure 4(d) shows the same phenomenon when the system is excited at 28 Hz, which is close to the second resonance. An additional peak appears around the frequency of the first mode. These results clearly demonstrate the mode interaction and energy transfer between the first two modes in the presence of the commensurable relationship in internal resonance.

With the validated equivalent circuit model, further simulations are performed to evaluate the power generated by the proposed harvester according to $P = V_{RL}{}^2/R_L$. Note that V_{RL} is the RMS value of the voltage across the resistive load R_L. Table II shows the power obtained by simulation at various excitation frequencies and resistive loads under the excitation with $a = 2\,\text{m/s}^2$. The underlined entries represent the optimal or near-optimal power. Though the exact optimal load varies with frequency, the resistance of 150 kΩ provides close to the optimal power over the frequency range around the resonances. Using this load, the frequency-sweep for the output power is conducted by simulation.

Figures 6(a) and 6(b) show the power outputs for up-sweep and down-sweep of the proposed internal resonance based nonlinear PVEH with various resistances and compared against the conventional linear configuration. At the power level of 100 μW, the proposed PVEH with optimal resistance (150 kΩ, solid black line) at $a = 2\,\text{m/s}^2$ provides a bandwidth of 2.65 Hz (downward sweep), which is a 130% increase compared to the bandwidth of 1.15 Hz of the linear harvester (dashed black line).

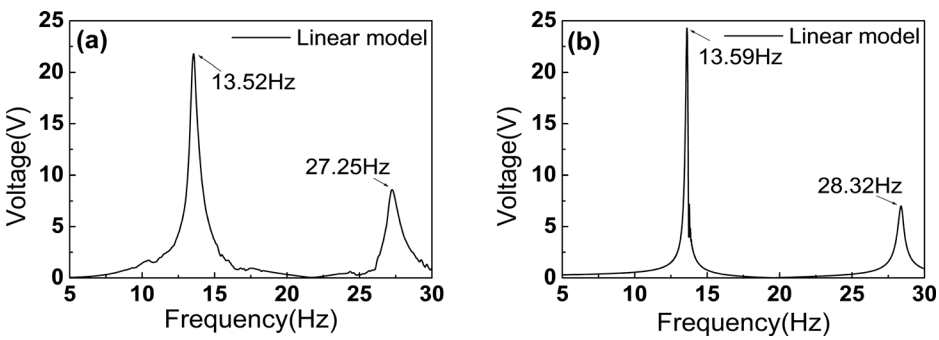

FIG. 3. Frequency responses of open circuit voltage of conventional linear energy harvester: (a) experiment and (b) simulation.

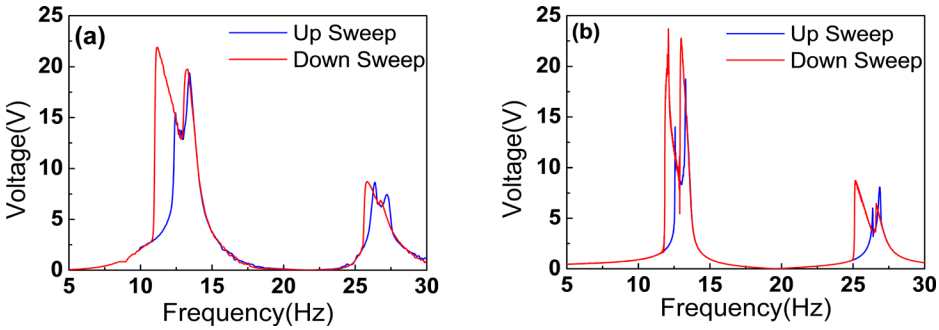

FIG. 4. Frequency responses of open circuit voltage of proposed nonlinear PVEH: (a) experiment and (b) simulation.

Figure 7 shows the power outputs of nonlinear PVEH away from internal resonance by varying the distance D_0 between the magnets. The resistance is also selected to be 150 kΩ. Only hardening or softening nonlinearity is demonstrated. The bandwidths over the power level of 100 μW for $D_0 = 9$ mm and $D_0 = 4.5$ mm are, respectively, 1.16 Hz and 1.36 Hz, which are wider than the linear configuration but narrower than the configuration with internal resonance. The improvement associated with the internal resonance mechanism is revealed.

In summary, this letter explores the application of internal resonance in enhancing energy harvesting. A prototype of a nonlinear 2DOF PVEH is conceptually designed. The linear auxiliary oscillator is introduced to easily attain commensurability of the natural frequencies and produce a 2:1 internal resonance. Both experiment and simulation capture the nonlinear characteristics of internal resonance and

TABLE II. Power (μW) obtained with different excitation frequencies and resistive loads. Underline indicates optimal or near-optimal powers and boldface indicates powers with optimal resistance 150 kΩ.

f(Hz) \ R_L(kΩ)	50	100	**150**	200	300	400
12.8	338	412	**457**	453	396	333
13.0	210	322	**352**	346	299	252
13.3	1109	1613	**1696**	1613	1337	1087
13.5	604	874	**920**	877	724	587
13.7	193	282	**298**	283	233	189
26.3	22.1	36.5	**42.7**	44.0	39.9	34.6
26.7	41.5	61.5	**65.6**	63.4	53.7	44.5
27.0	200	283	**288**	268	219	178
27.1	128	175	**173**	155	121	96.6
29.0	4.44	5.87	**5.64**	4.98	3.81	3.00

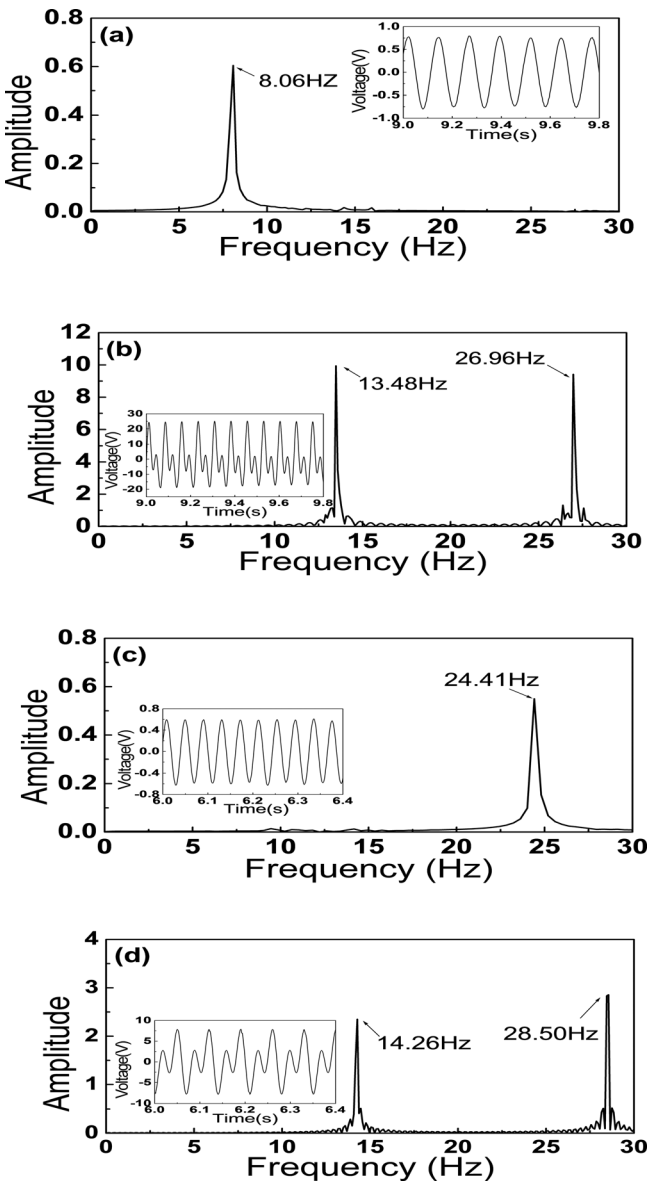

FIG. 5. Response spectrum with different excitation frequencies: (a) 8 Hz, (b) 13.5 Hz, (c) 24 Hz, and (d) 28 Hz.

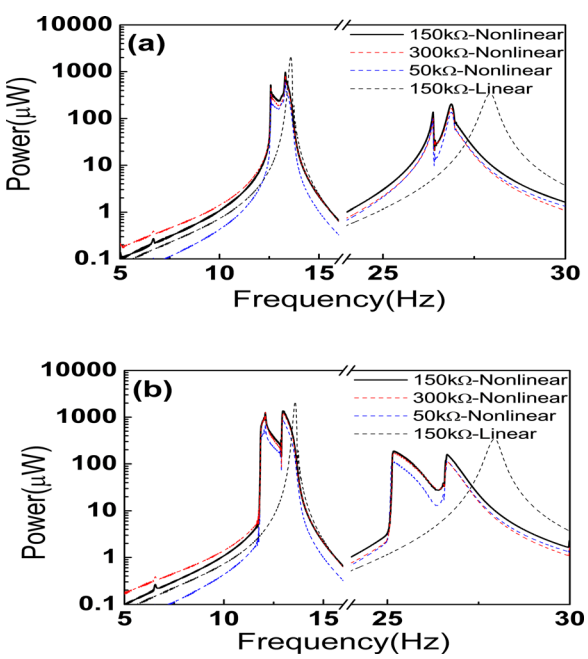

FIG. 6. Simulation results of power outputs comparing linear PVEH and nonlinear PVEH with internal resonance: (a) up sweep and (b) down sweep.

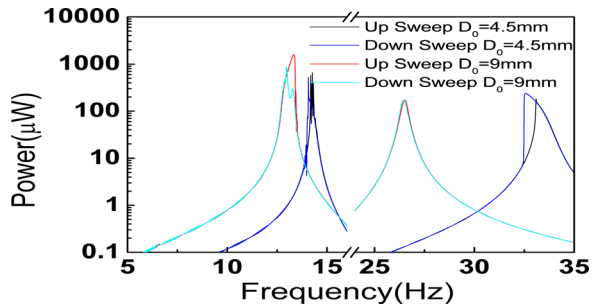

FIG. 7. Simulation results of power outputs of nonlinear PVEH away from internal resonance.

demonstrate their exciting potential to broaden the operating bandwidth.

[1]H. A. Sodano, G. Park, and D. J. Inman, Strain **40**, 49 (2004).
[2]L. Gammaitoni, I. Neri, and H. Vocca, Appl. Phys. Lett. **94**, 164102 (2009).
[3]A. Erturk and D. J. Inman, *Piezoelectric Energy Harvesting* (John Wiley & Sons, Atlanta, 2011).
[4]L. H. Tang and Y. W. Yang, Appl. Phys. Lett. **101**, 094102 (2012).
[5]J. Y. Cao, S. X. Zhou, and D. J. Inman, Appl. Phys. Lett. **107**, 143904 (2015).
[6]S. Roundy and Y. Zhang, Proc. SPIE **5649**, 373 (2005).
[7]M. Lallart, S. R. Anton, and D. J. Inman, J. Intell. Mater. Syst. Struct. **21**, 897 (2010).
[8]Q. Ou, X. Q. Chen, S. Gutschmidt, A. Wood, N. Leigh, and A. F. Arrieta, J. Intell. Mater. Syst. Struct. **23**, 117 (2012).
[9]M. Arafa, W. Akl, A. Aladwani, O. Aldrarihem, and A. Baz, Proc. SPIE **7977**, 79770Q (2011).
[10]S. M. Shahruz, J. Sound Vib. **292**, 987 (2006).
[11]M. Ferrari, V. Ferrari, M. Guizzrtti, D. Marioli, and A. Taroni, Sens. Actuators, A **142**, 329 (2008).
[12]A. Aladwani, M. Arafa, O. Aldraihem, and A. Baz, J. Vib. Acoust. **134**, 031004 (2012).
[13]H. L. Liu, Z. Y. Huang, T. Z. Xu, and D. Y. Chen, Smart Mater. Struct. **21**, 065004 (2012).
[14]A. Erturk, J. M. Renno, and D. J. Inman, J. Intell. Mater. Syst. Struct. **20**, 529 (2009).
[15]L. H. Tang and Y. W. Yang, J. Intell. Mater. Syst. Struct. **23**, 1631 (2012).
[16]H. Wu, L. H. Tang, Y. W. Yang, and C. K. Soh, Jpn. J. Appl. Phys., Part 1 **51**, 040211 (2012).
[17]A. F. Arrieta, P. Hagedorn, A. Erturk, and D. J. Inman, Appl. Phys. Lett. **97**, 104102 (2010).
[18]S. D. Nguyen and E. Halvorsen, J. Microelectromech. Syst. **20**, 1225 (2011).
[19]A. Erturk and D. J. Inman, J. Sound Vib. **330**, 2339 (2011).
[20]F. Cottone, H. Vocca, and L. Gammaitoni, Phys. Rev. Lett. **102**, 080601 (2009).
[21]S. C. Stanton, C. C. McGehee, and B. P. Mann, Appl. Phys. Lett. **95**, 174103 (2009).
[22]L. Q. Chen, G. C. Zhang, and H. Ding, J. Sound Vib. **354**, 196 (2015).
[23]L. Q. Chen and W. A. Jiang, J. Appl. Mech. **82**, 031004 (2015).
[24]C. B. Lan, W. Y. Qin, and W. Z. Deng, Appl. Phys. Lett. **107**, 093902 (2015).
[25]J. Xu and J. Tang, Appl. Phys. Lett. **107**, 213902 (2015).
[26]D. X. Cao, S. Leadenham, and A. Erturk, Eur. Phys. J.-Spec. Top. **224**, 2867 (2015).
[27]E. Engel, J. Y. Wei, and C. L. Lee, Proc. SPIE **9493**, 94930Q (2015).